# Dual Cavity Dielectric Modulated Ferroelectric Charge Plasma Tunnel FET As Biosensor: For Enhanced Sensitivity

Shradhya Singh, Sangeeta Singh, *Member, IEEE,* Mustafa K. A. Mohammed*, and Girish Wadhwa, *Member, IEEE,*

***Abstract*—This work reports a biosensor based on the dual cavity dielectric modulated ferroelectric charge plasma Tunnel FET (FE-CP-TFET) with enhanced sensitivity. By incorporating underlap and dielectric modulation phenomena, ultra sensitive, and label-free detection of biomolecules is achieved. The cavity is carved underneath the source-gate dielectric for the immobilization of the biomolecules. The ferroelectric (FE) material is used as a gate stack to realize a negative capacitance effect to amplify the low gate voltage. To avoid the issues with metallurgical doping such as random dopant fluctuations (RDFs), ambipolar conduction, and increased thermal budget, the charge plasma concept is deployed. Based on our exhaustive ATLAS 2D TCAD study, the electric field, hole concentration, and energy band diagram of the proposed device are critically analyzed to provide a better insight into the biosensor working mechanism. Here, two different figures-of merits (FOMs) for the proposed biosensor are investigated such as sensitivity and linearity. Sensitivity has been measured in terms of drain current, $I_{ON}$ to $I_{OFF}$ ratio, electric field, and transconductance sensitivity. Linearity analysis of the proposed structure includes $I_{ON}/I_{OFF}$ ratio. The reported biosensor is capable of detecting several biomolecules such as (neutral and charged as well) Streptavidin (2.1), 3-aminopropyltriethoxysilane (APTES)(K = 3.57), Keratin (K = 8), T7 (K = 6.3) and Gelatin (K = 12). It was observed that the optimized cavity structure demonstrates high drain current sensitivity (2.7$\times 10^8$) as well as high $I_{ON}/I_{OFF}$ sensitivity (1.45$\times 10^8$). Further, the linearity analysis shows that the Pearson's coefficient of both structures have been achieved as ($r^2 \geq$ 0.8). It is conferred from the results that our biosensor can be a better alternative for the detection of the various neutral and charged biomolecules.**

***Index Terms*—Dielectric Modulated TFET, Ferroelectric, Negative capacitance, Biosensor, Figure-of-merit (FOM).**

## I. Introduction

RECENTLY, dielectric modulated biosensors based on field-effect transistors have drawn considerable attention among researchers for the label-free detection of biomolecule species. Early-stage identification of bioanalytes without using costly probes and composites can not be possible with the labeled detection methods due to its inaccurate results and time consuming labeling process [1]- [3] like optical [4], electrochemical [5], and magnetic [6] etc. Therefore, dielectric modulated FET based biosensors have become an interesting candidate for the research owing to their integration with CMOS technology, label-free detection, scalability, low cost, small size, enhanced sensitivity, and compatibility with other electronic gadgets for the applications of system-on-chip (SoC) [7], [8]. The applications of biosensors are in various domains such as environment condition monitoring, food industry, medical field, biospecies analysis, etc. [9]-[11]. The speed of detection and sensitivity are the two most important factors of the biomolecule detection system [12], [13]. The past research studies and analyses the dielectric modulated MOSFET [14]- [17]. In dielectric modulated FETs, the binding sites for biomolecules are formed under the gate electrode or towards drain/source ends. Biomolecules having different dielectric constant values (K) get trapped in the cavity region tune the electrical characteristics i.e., threshold voltage and/or drain current. This acts as a critical metric for the detection property of dielectric modulated FETs.

In the meantime, for achieving the demands of advanced technology such as minimum power consumption, enhanced speed, increased packing density, etc., miniaturization of device dimensions is mandatory. However, due to several unavoidable difficulties such as short channel effects (SCEs), high leakage current, high power consumption, and deteriorating $I_{ON}/I_{OFF}$, the scaling of conventional CMOS technology has hindered the semiconductor industry's advancement. Therefore, tunnel field effect transistor TFET has been investigated as a viable alternative due to its ability to survive the negative effects of downscaling and has a reduced leakage current and subthreshold slope (SS) below Boltzmann's limit (60mV/decade). The literature has also reported that the maximum sensitivity of MOSFETs is also restricted by the larger response time and degradable SS. Furthermore, due to the intrinsic phenomena of band-to-band tunneling, the limitations of MOSFET-based biosensors may be successfully resolved by deploying TFET-based biosensors. This leads to a superior SS and, as a result, stronger sensitivity and faster response time [14], [18], [19].

Although TFETs have outperformed CMOS still they have major limitations in terms of ON-state current and ambipolar conduction [20], [21]. To overcome these problems, various modified TFET structures have been reported. It includes gate metal work function engineering, multigate TFET, hetero-dielectric TFET, the introduction of low bandgap material

Shradhya Singh and Sangeeta Singh are with Microelectronics & VLSI lab, National Institute of Technology, Patna-800005, India.
(e-mail: shradhyasingh92@gmail.com; sangeetasingh.1409@gmail.com)
Mustafa K. A. Mohammed is with Radiology Techniques Department, Dijlah University College, Al-Masafi Street, Baghdad, Iraq. (email: mustafa_kareem97@yahoo.com)
Girish Wadhwa is with Dr. B. R. Ambedkar NIT Jalandhar, Punjab-144805, India. (e-mail: girishw.17.phd@nitj.ac.in)
* Corresponding Author

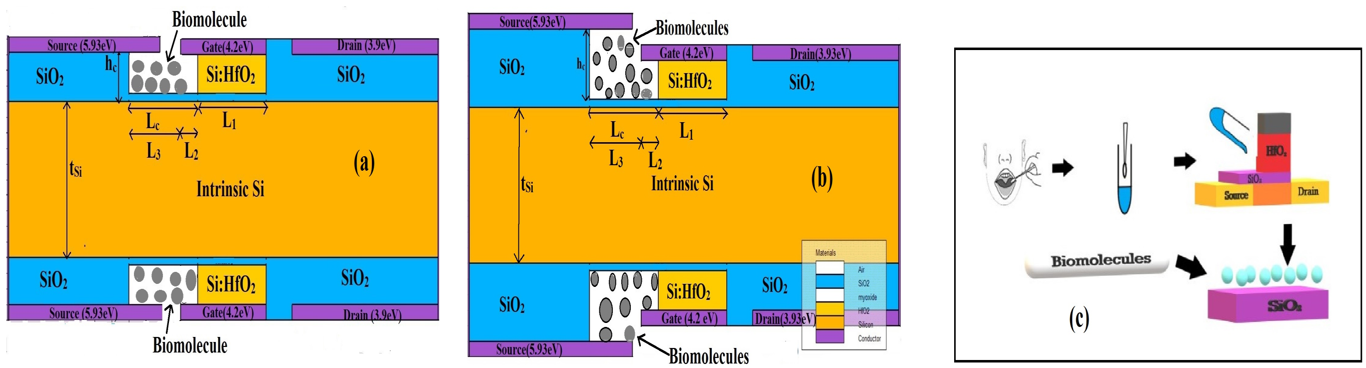


Fig. 1: 2-D schematics of FE-CP-TFET based biosensor (a) with cavity height $h_c$ = 2.5 nm and (b) with cavity height $h_c$ = 5.5 nm (c) biomolecules immobilization model.

towards source side, vertical TFET [22]- [25], the introduction of negative capacitance (NC) with ferroelectric (FE) material as gate dielectric [26]. In 2010, first-time ferroelectric tunnel FET (FE-TFET) was proposed by Lattanzio and his research group [26], and it boosts the drain current and transconductance with a maximum near or beyond the Curie temperature with the ferroelectric gate stack at elevated temperatures and achieved step SS by utilizing the principle of P(VDE-TrFE). Different studies on the impact of scaling [27], various structural improvements on electrical parameters in terms of $I_{ON}/I_{OFF}$ ratio, memory window, and SS have been carried out so far [28]- [31], but the deployment of ferroelectric TFET as a biosensor has not been explored yet.

The tunneling efficiency at lower bias points must be enhanced to retain the inherent benefits of a TFET. The electric field at the tunnel junction is greatly enhanced when negative gate stack capacitance has been introduced. The use of ferroelectric insulator in the gate-stack with conventional oxide gives negative capacitance (NC) effect and works as a step-up voltage transformer due to intrinsic voltage amplification, providing excellent ON-current and steep SS [53]. For the conventional TFET SS can be expressed as [54]:

$$SS = ln10\left[\frac{1}{V_{eff}}\frac{dV_{eff}}{dV_{gs}} + \frac{E+b}{E^2}\frac{dE}{dV_{gs}}\right]^{-1} \tag{1}$$

Where, the effective bias of tunneling junction is represented by $V_{eff}$, b is material constant, E shows electric field. d$V_{gs}$/d$V_{eff}$ is defined by the capacitive voltage divider in such a manner:

$$\frac{dV_{gs}}{dV_{eff}} = 1 + \frac{C_s}{C_{ins}} \tag{2}$$

where $C_{ins}$ is measured as the equivalent capacitance of series capacitances of the gate oxide capacitance $C_{ox}$ and ferroelectric insulator capacitance $C_{ferro}$. The ferroelectric layer serves as a step-up transformer due to NC, resulting in $V_{eff} > V_{gs}$. Furthermore, positive feedback effect on the charge (Q) of the capacitor owing to NC may be understood as the internal voltage amplification in CP-FE-TFET that improves the electric field at tunnel junction. Consider a (positive) capacitor $V_{gs}$ (per unit area) with a terminal voltage equal to the applied voltage $V_{gs}$ plus a feedback voltage $\beta_F$Q proportional to the charge on the capacitor Q (per unit area):

$$Q = C_g\left((V_{gs} - V_{eff}) + \beta_F Q\right) \tag{3}$$

and now $C_{ins}$ can be expressed as

$$C_{ins} = \frac{Q}{V_{gs} - V_{eff}} = \frac{C_g}{1 - \beta_F C_g} \tag{4}$$

According to Eqn. (1), the negative gate-stack capacitance ($C_{ins}$) can only be formed when the feedback voltage is greater than one (i.e. ($\beta_F$Q $>$ 1))). According to Eqns. (2) and (4), a positive feedback is the result of NC to step-up the internal voltage at the tunnel junction:

$$\frac{dV_{gs}}{dV_{eff}} = 1 - \frac{C_s}{C_{ins}}\left(\,\beta_F C_g - 1\right) \tag{5}$$

Due to positive feedback voltage ($\beta_F Q$ >1), $dV_{gs}/dV_{eff}$ decreases. Thus, it is evident from Eqn. (1) and Eqn. (5) that SS depends on Eqn.(5) factor, as evident from Eqn. (1) that SS reduces drastically.

Improvement in the ON-state current can be achieved by increasing the electron tunneling rate owing to enhanced carrier concentration beneath the gate dielectric i.e., channel region. This can be done by having a higher doping concentration towards the source side in comparison with the drain side [32], [33]. But, the source doping concentration is limited to $1{\times}10^{20}cm^{-3}$ due to the solid solubility limit, and also a high thermal budget is required for establishing the source and drain region. By avoiding metallurgical doping, these issues and fabrication complexities can be addressed [35], [36]. As a result, the charge-plasma approach has been devised to form the source and drain regions in TFETs by depositing suitable metal with appropriate work functions on each side [36]-[38].

Therefore, by an extensive review of available literature report, for the very first time, a novel TFET structure-based biosensor has been proposed by combining the utility of charge plasma technique and negative capacitance effect. Thus, in this work, a dual cavity dielectric modulated ferroelectric charge plasma Tunnel FET (FE-CP-TFET) based biosensor has been investigated for the label-free biomolecule detection with two

TABLE I: Simulation parameters for negative capacitance charge plasma TFET (FE-CP-TFET) based biosensor with cavity height $h_c$ = 2.5 nm and $h_c$ = 5.5 nm.

| Parameters | Structure 1 | Structure 2 |
|---|---|---|
| Silicon thickness ($T_{Si}$ ) | 10 nm | 10 nm |
| Gate-oxide thickness($T_{ox}$) | 2.5 nm | 2.5 nm |
| Gate length($L_G$ = $L_1$+$L_2$) | 40 nm+10 nm | 40 nm+10 nm |
| Source length ($L_S$) | 100 nm | 100 nm |
| Drain length ($L_D$) | 100 nm | 100 nm |
| Background doping ($N_{in}$) | $1 \times 10^{16} cm^{-3}$ | $1 \times 10^{16} cm^{-3}$ |
| Source work-function( $\phi_S$ (Pt)) | 5.93 eV | 5.93 eV |
| Drain work-function($\phi_D$ (Hf)) | 3.9 eV | 3.9 eV |
| Gate Dielectric constant ($\epsilon_{ox}$) | $HfO_2$ (31) | $HfO_2$ (31) |
| Cavity thickness ($h_c$) | 2.5 nm | 5.5 nm |
| Cavity Length ($L_c$ = $L_2$ + $L_3$) | 10 nm + 30 nm | 10 nm + 30 nm |

TABLE II: Different biomolecules with its dielectric constants (K) [14]-[17].

| Biomolecules | Dielectric constant (K) |
|---|---|
| Streptavidin | 2.1 |
| 3-aminopropyltriethoxysilane (APTES) | 3.57 |
| Bacteriophage T7 | 6.3 |
| Keratin | 8 |
| Gelatin | 12 |

etched nanogap cavities in the source-gate dielectric interfaces. It overcomes the limitation of solid solubility and also leads to the enhanced carrier concentration in the channel region. A thin coating of $SiO_2$ has been grown in the cavity region as an adhesive layer to bind the immobilized bioanalytes, which needs to be detected. The proposed device can be utilized to detect both neutral as well as charged biomolecules. The immobilized biomolecules within the cavity region alter the gate oxide capacitance and consequently vary the flat band voltage, which is reflected in the device's electrostatic profile. For examining the device performances energy band gap, surface potential, electric field, and transfer characteristics of the reported biosensor with various biomolecules immobilization such as Streptavidin, APTES, T7, Keratin, and Gelatin are analyzed to test the target biomolecules. The proposed device has the cavity thickness of 2.5 nm and 5.5 nm to immobilize the biomolecule accurately. It has been studied that the thickness and length of the biomolecules are below 2 nm and 5 nm respectively. Finally, drain current sensitivity is measured with the variation of different dielectric constants (K) and charge densities ($N_f$) of the target biomolecules [18]-[20].

This paper is structured in four parts. Section II refers to the device architecture and simulation parameters used for the analysis of the proposed device structure. Results are discussed in part III and part IV presents the conclusion.

## II. DEVICE ARCHITECTURE AND SIMULATION APPROACH

Fig. 1 depicts the transversal section of dual cavity dielectric modulated ferroelectric charge plasma Tunnel FET (FE-CP-TFET) based biosensor with cavity height ($h_c$ = 2.5 nm) structure 1 as shown in Fig. 1(a) and $h_c$ = 5.5 nm structure 2 as illustrated in Fig. 1(b). Fig. 1(c) represents the model for biomolecule immobilization in the nanocavity areas of the

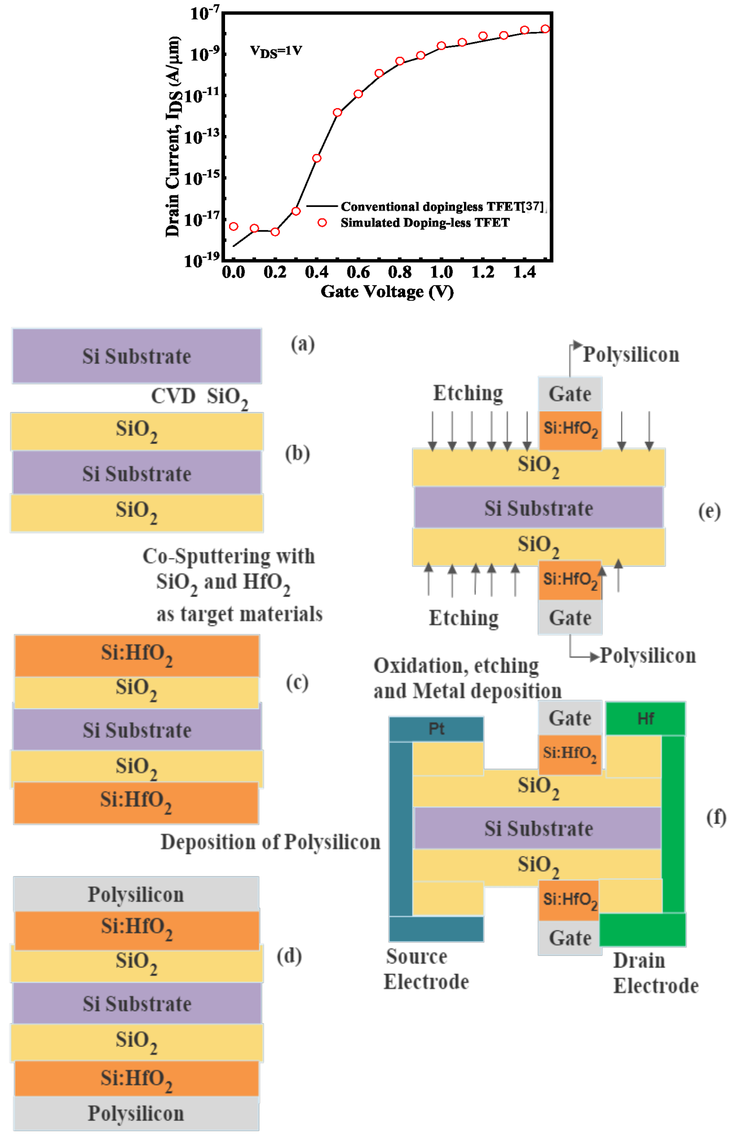


Fig. 2: (a) Calibration of simulation model with pre-fabricated TFET, and (b) Proposed process flow for the probable fabrication of FE-CP-TFET.

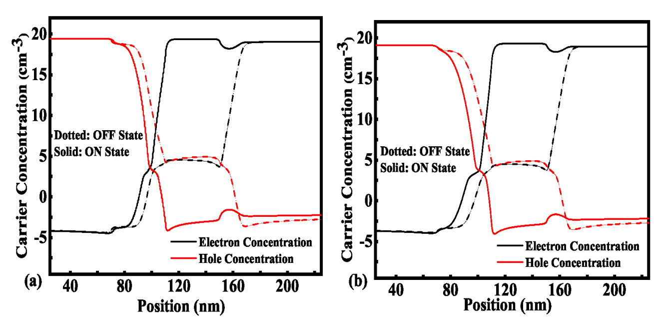


Fig. 3: Electron and hole concentrations of FE-CP-TFET based biosensor (a) with cavity height $h_c$ = 2.5 nm and (b) with cavity height $h_c$ = 5.5 nm.

proposed structure. It has been utilized to identify the presence of bio-analytes with the effect of the dielectric modulation

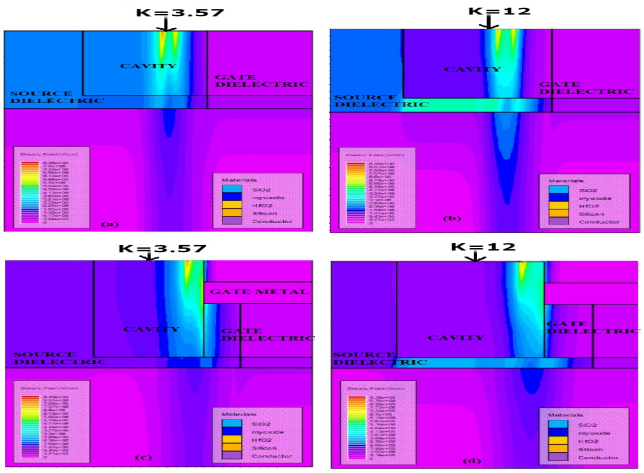


Fig. 4: 2-D Electric field distribution in FE-CP-TFET based biosensor (a) with cavity height $h_c$ = 2.5 nm of biomolecules (K = 3.57); (b) with cavity height $h_c$ = 2.5 nm of biomolecules (K = 12); (c) with cavity height $h_c$ = 5.5 nm of biomolecules (K = 3.57); and (d) with cavity height $h_c$ = 5.5 nm of biomolecules (K = 12).

approach. Underlap opening in the source-gate dielectric acts as the binding region for the interlinkage of the biomolecules with the device. The creation of the nanocavity region at the source-gate dielectric results in improved performance, suppression of ambipolarity, and leakage current. Here, Si-doped Hf$O_2$ FE material is utilized for the gate stacking with convention oxide for the intrinsic amplification of the low gate voltages to enable the low power application. The detailed FE material parameters of Si:Hf$O_2$ considered for the device simulations are coercive field ($F_C$), remanent polarization ($P_r$), saturation polarization ($P_s$), and the dielectric constant of doped Si:Hf$O_2$ (FE) are considered to be 1 MV/cm, 1 $\mu$C/$cm^2$, 20 $\mu$C/$cm^2$, and 31, respectively [27]. The charge plasma technique is utilized to create source and drain region to avoid several fabrication complexities such as higher thermal budget, random dopant fluctuations (RDFs), mobility degradation, etc. It is created by forming drain and source regions with appropriate metals having acceptable work functions, such as Hf (3.9 eV) and Pt (5.93 eV), respectively. The length of the gate dielectric below the gate metal has two regions: region 1 with length $L_2$ consists of a gate underlap region to act as a binding site for the biomolecules and region 2 consists of the gate dielectric with length $L_1$. Total cavity length extended underneath source and gate metal with the lengths $L_3$ and $L_2$, respectively. Detailed device dimensional parameters taken are listed in TABLE. I.

The simulation frame work deployed here for the analysis of dopingless TFET has been calibrated against the reported data [37] as shown in Fig. 2(a) and it shows good agreement with reported data. As doping less concept experimentally realized only for diode not for the TFET. Thus, for deploying the doping less concept, we have calibrated our simulation frame work against [37]. During the fabrication of the dual cavity dielectric modulated FE-CP-TFET based biosensor, the cavity region can be developed in source-gate dielectric by dry etching. A thin layer of Si$O_2$ is grown on the Si film by CVD in the cavity region, which acts as an adhesive layer for bio-targets. Then desired thin film of Si doped Hf$O_2$ could be co-sputtered over the adhesive Si$O_2$ layer with Si$O_2$ and Hf$O_2$ targets as a switching layer. It has been discovered that when a thin layer of Si doped Hf$O_2$ is developed under mechanical encapsulation, an orthorhombic phase is formed, which exhibits the piezoelectric response. This phase has been determined to be ferroelectric by polarization measurements [50], [51]. Metalization of the gate, source, and drain region can be achieved by low-pressure chemical vapor deposition (CVD) [38]. The detailed process flow that could be deployed for the potential fabrication of the reported biosensor are shown in Fig. 2 (b). The performance assessment of the dual cavity dielectric modulated ferroelectric charge plasma tunnel FET (FE-CP-TFET) based biosensor is done by immobilizing the cavity region completely with different biomolecules. In this, neutral biomolecules has the dielectric constant (K) and charged biomolecule consists of the charge density ($N_f$) and dielectric constant both. For the validation of the proposed structure as a biosensor, different biomolecules with the universally accepted dielectric constant values have been considered. Bioanalytes such as Streptavidin (used for detection of proteins, nucleic acids and lipids), 3-aminopropyltriethoxysilane (APTES, utilized for silanization), Bacteriophage T7 (it can kill various advantageous bacteria), Keratin, and Gelatin (proteins that can float in skin, hair, and nails) has been utilized for examining the proposed device as a biosensor and the corresponding values of their dielectric constants are mentioned in TABLE II.

To investigate the performance of the proposed structure i.e., dual cavity dielectric modulated ferroelectric charge plasma Tunnel FET (FE-CP-TFET) based biosensor, 2D device simulator in commercially available ATLAS TCAD SILVACO tool version 2020 [39] has been utilized. Different device models have been induced in the simulator to achieve precise simulation of device parameters. The non-local BTBT model is used to calculate the tunneling rate at the tunneling junction [14]- [16]. The CVT model is used to incorporate mobility that is depending on field and concentration. The Shockley-Read-Hall (SRH) model is used to account for carrier recombination. To allow for the high concentration impact on the bandgap, the band gap narrowing (BGN) model is chosen [35]- [36]. While the simulation of the device, Ferro model is used to accommodate the silicon doped Hf$O_2$ material for its ferroelectric properties. A ferroelectric miller model is considered to account for the hysteresis, polarization, and high-K of the ferroelectric material [49].

## III. RESULT AND DISCUSSION

In this section, to estimate the utility of the device three different kinds of figure of merits (FOM) have been investigated. It includes sensitivity and linearity analysis of the proposed structure. The response of the proposed structures has been examined as a biosensor for both neutral as well as charged biomolecules. The sensitivity performance of the device has been evaluated by substituting the air with K = 1 in the cavity region under the source-gate dielectric by the biomolecules as mentioned in TABLE. II. The dielectric value of the neutral biomolecules varies from K = 1 to K = 12 and the charge density of the charged biomolecules varies from $N_f = \pm 10^{10}$ to $N_f = \pm 10^{12}$. Firstly, electrostatic analysis of the proposed structures has been investigated.

### A. Electrostatic analysis of FE-CP-TFET based biosensor

The charge carriers concentrations of the proposed devices (1 nm below the Si-Si$O_2$ interface) are illustrated in Fig. 3. It should be emphasized that despite the lack of metallurgical doping, both devices were able to obtain the needed carrier concentration profiles by using the charge plasma approach to actualize the $p^+ - i - n^+$ region. Because the structures under consideration are double gate, the tunneling rates at both interfaces are similar. According to the equation, the tunneling rate $G_{BTBT}$ in a TFET structure is a function of the local electric field (EF) [40]:

$$G_{BTBT} = AE^{\sigma} exp \left( -\frac{B}{E} \right) \tag{6}$$

In Eqn. (6), constant $A$ depends upon the electron's effective mass its value is $4\times 10^{14} V^{-2} S^{-1} cm^{-1}$, $B$ represents the tunneling probability constant (30MV/cm), $\sigma$ indicates the transition constant (2.5 for Si) [52]. Fig. 4 illustrates the distribution of 2D electric field in negative capacitance charge plasma TFET (FE-CP-TFET) based biosensor of both the cavities height structures. For analyzing the impact of dielectric constants of the target biomolecules in the cavity region on electric field distribution, K = 3.57 and K = 12 values have been chosen. It can be noted from the figure that at the higher K values the electric field increases significantly owing to the better capacitance coupling between the gate and the channel region. Fig. 5 depicts the variation in hole carrier concentration beneath the cavity region with respect to the variation in the dielectric constant of the bio-analyte considered to be detected.

It is also depicted in Fig. 5(a) and Fig. 5(b). The presence of charged biomolecules in the cavity region affect the hole concentrations of the source region as depicted in Fig. 5 (c) and 5(d). It can be stated that when the trapped biomolecules in the cavity region is negatively charged, it attracts more number of charge carriers (holes) in the source region resulting in the steepness at the tunneling junction. The opposite phenomenon happens for positively charged biomolecules. The tunneling probability in the TFET structure is expressed by Wentzel-Kramer-Brillouin (WKB) approximation (TWKB) and is defined as Eqn. (7) and (8) [41];

$$T_{WKB} = exp \left( -\frac{4\lambda\sqrt{2m^*}\sqrt{E_g^3}}{3q\hbar \left( E_g + \Delta\phi \right)} \right) \tag{7}$$

$$\lambda = \sqrt{\frac{\epsilon_{Si}}{\epsilon_{bio}} h_c t_s} \tag{8}$$

Here, $m^*$ shows the effective mass of the electron, $E_g$ shows the energy band gap, and $\Delta\phi$ is defined as the range of energy for which the tunneling can take place and $\lambda$ represents the screening tunneling width. It depends on $h_c$ which represents the cavity height under source gate dielectric, $t_s$ is Si body thickness, $\epsilon_{bio}$ represents the dielectric constant of biomolecules immobilized in the cavity region and $\epsilon_s$ is the dielectric constant of Si semiconductor. To understand the $T_{WKB}$ in the proposed structure, here an analysis of the variation in the energy band diagram along the cut-line i.e. below the 1 nm of $SiO_2$-Si interface under the presence of different biomolecules at the binding sites are illustrated in Fig. 6. It shows that an increase in dielectric constant reduces the tunneling barrier width at the source channel junction due to the enhancement in the hole concentration and results in the maximum tunneling rate at K=12. Positively charged biomolecules trapped in the cavity region attracts the electrons, hence the reduction of the hole concentration towards the source region leads to the widening of the tunneling barrier. Whereas, narrower tunneling width can be observed for the negatively charged biomolecules. In other words, band bending of the structure is achieved at a higher value of K as the enhanced electric field can be observed at high K value as shown in Fig. 7 along the same cut-line. The immobilization of the biomolecules in the cavity region causes the sharp doping profile as the dielectric values increases in the cavity resulting in the enhanced electric field at the tunneling junction. The maximum electric field of 2.13× $10^6$ V/cm has been achieved at the tunneling junction for K=12 for structure 1 and 1.88× $10^6$ V/cm for structure 2.

The drain current variations with gate to source voltage at $V_{DS}$ = 1 V in both devices of (FE-CP-TFET) based biosensor are illustrated in Fig. 8. The variations in transfer characteristics are obtained for different neutral biomolecules with corresponding dielectric constants ranging from K = 2.1 to K = 12. It can be noted that with an increase in dielectric constant the hole carrier density gets enhanced under the source cavity region resulting in the modulation of tunneling barrier width. Hence, an increase in $T_{WKB}$ leads to a higher ON current. Fig. 8(a) and (b) describe the impact of neutral biomolecules with K value on the transfer characteristic of the biosensor. It can be seen that the maximum peak is achieved as 3.77 $\times 10^{-8}$ A/$\mu$m at K = 12. The impacts of the positively charged (with charge density $N_f = 10^{10} cm^{-2}$ to $N_f = 10^{12} cm^{-2}$) biomolecules trapped in the cavity region on transfer characteristic are described in Fig. 8(c) and 8(d) for both the structures. The increment of the positively charged biomolecules concentrations in the cavity region leads to the reduction of hole carrier concentration, which results in the reduction of ON current. Hence, there is a degradation of drain current, which can be observed in Fig. 8(c) and 8(d). On other hand, the presence of negatively charged biomolecules (with charge density $N_f = -10^{12} cm^{-2}$ to $N_f = -10^{10} cm^{-2}$ ) in the cavity region, attracts a large number of holes. Thus, the improvement in the majority carrier concentration at the source region narrower the tunneling barrier width and enhances the tunneling rate. Hence, elevation in the $I_{ON}$ with negatively charged biomolecules is portrayed in Fig. 8(e) and 8(f). Fig. 9 indicates the impact of dielectric modulation of neutral biomolecules in the cavity region on the RF parameter i.e.

This article has been accepted for publication in a future issue of this journal, but has not been fully edited. Content may change prior to final publication. Citation information: DOI 10.1109/TNB.2022.3174266, IEEE Transactions on NanoBioscience



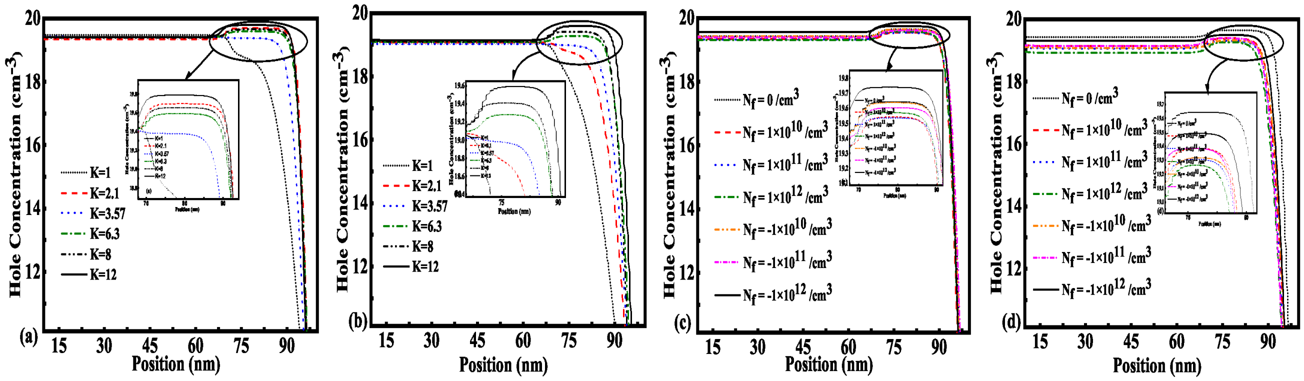


Fig. 5: Hole concentration of FE-CP-TFET based biosensor for (a) neutral biomolecule with cavity height $h_c$ = 2.5 nm; (b) neutral biomolecule with cavity height $h_c$ = 5.5 nm; (c) charged biomolecule with cavity height $h_c$ = 2.5 nm and (d) charged biomolecule with cavity height $h_c$ = 5.5 nm.

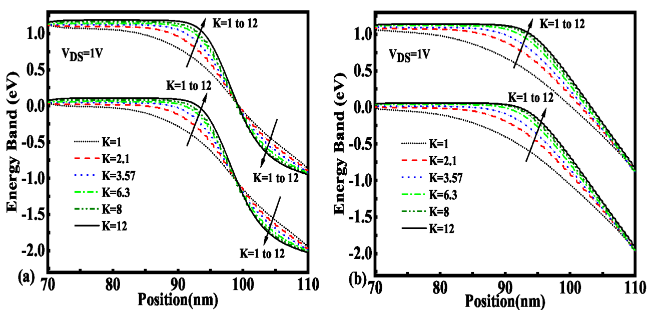


Fig. 6: Energy band diagram of FE-CP-TFET based biosensor (a) with cavity height $h_c$ = 2.5 nm and (b) with cavity height $h_c$ = 5.5 nm.

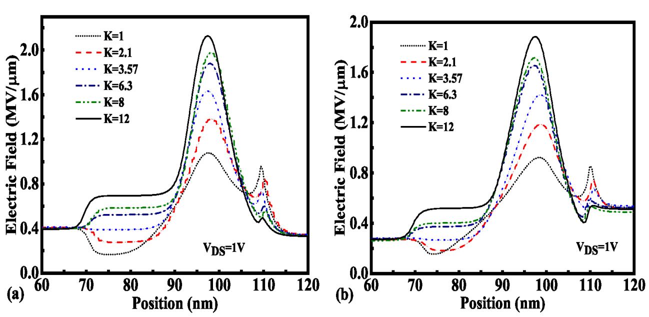


Fig. 7: Electric field of FE-CP-TFET based biosensor (a) with cavity height $h_c$ = 2.5 nm and (b) with cavity height $h_c$ = 5.5 nm.

transconductance ($g_m$) of the proposed devices, is defined as $g_m = dI_D/dV_{GS}$. As an increase in K value improves the drain current, hence transconductance of both the devices increase. The maximum value of transconductance is achieved as $3.56\times10^{-7}$ s/$\mu$m and $1.64\times10^{-8}$S/$\mu$m for the both the proposed structures respectively.

### B. Sensitivity analysis of FE-CP-TFET based biosensor

Sensitivity is an essential FOM to evaluate the performance of a biosensor. Thus, to accurately detect the biomolecules to be targeted, the sensitivity of the device should be as high as possible. However, highly sensitive biosensors have also suffered from the problem of selectivity and specificity which may result in a false positive response from a negative sample. The sensitivity of the FE-CP-TFET based biosensor is computed, which is centered on the change in drain current, electric field sensitivity, change in $I_{ON}/I_{OFF}$ ratio and transconductance sensitivity is considered a key sensing metric, which can sense the existence of the charged as well as neutral biomolecules immobilized within the cavity precisely. Sensitivity is defined as [25]:

$$S_{I_D} = \left( \frac{I_D\,(bio) - I_D\,(air)}{I_D\,(air)} \right) \tag{9}$$

In Eqn. (9), $I_D(bio)$ represents the drain current corresponding to the completely filled cavity and empty cavity yield the drain current as $I_D(air)$.
The presence of neutral biomolecules in the source-channel dielectric cavity region the capacitive coupling between the gate metal with the channel and the source metal with source region gets enhanced resulting in an increment in the drain current. Fig. 10 (a) and 10(b) demonstrate the drain current sensitivity of FE-CP-TFET based biosensor with cavity height $h_c$ = 2.5 nm and $h_c$ = 5.5 nm, respectively with the neutral biomolecules having a corresponding dielectric constant ranging from K = 2.1 to K = 12. It is revealed that the improvement in drain current sensitivity has been achieved with an increased K value of neutral biomolecules. The maximum drain current sensitivity of the proposed structure with cavity height of $h_c$ = 2.5 nm achieved by the proposed model is 5.92 $\times10^7$ for K = 12 at $V_{GS}$ = 0.8 V and with the cavity height of $h_c$ = 5.5 nm, 2.76 $\times10^8$ for K = 12 at $V_{GS}$ = 1 V.

The impact of variation in the dielectric value (K) with the presence of different neutral biomolecules in the cavity region on the electric field sensitivity of the proposed structures is depicted in Fig. 11. It is noted that the $E_F$ increases with the K value as already mentioned in Fig. 7 resulting in improved $E_F$ sensitivity at the elevated value of K. At K = 12, the maximum $E_F$ sensitivity is achieved for 3.2 and 2.3 for both

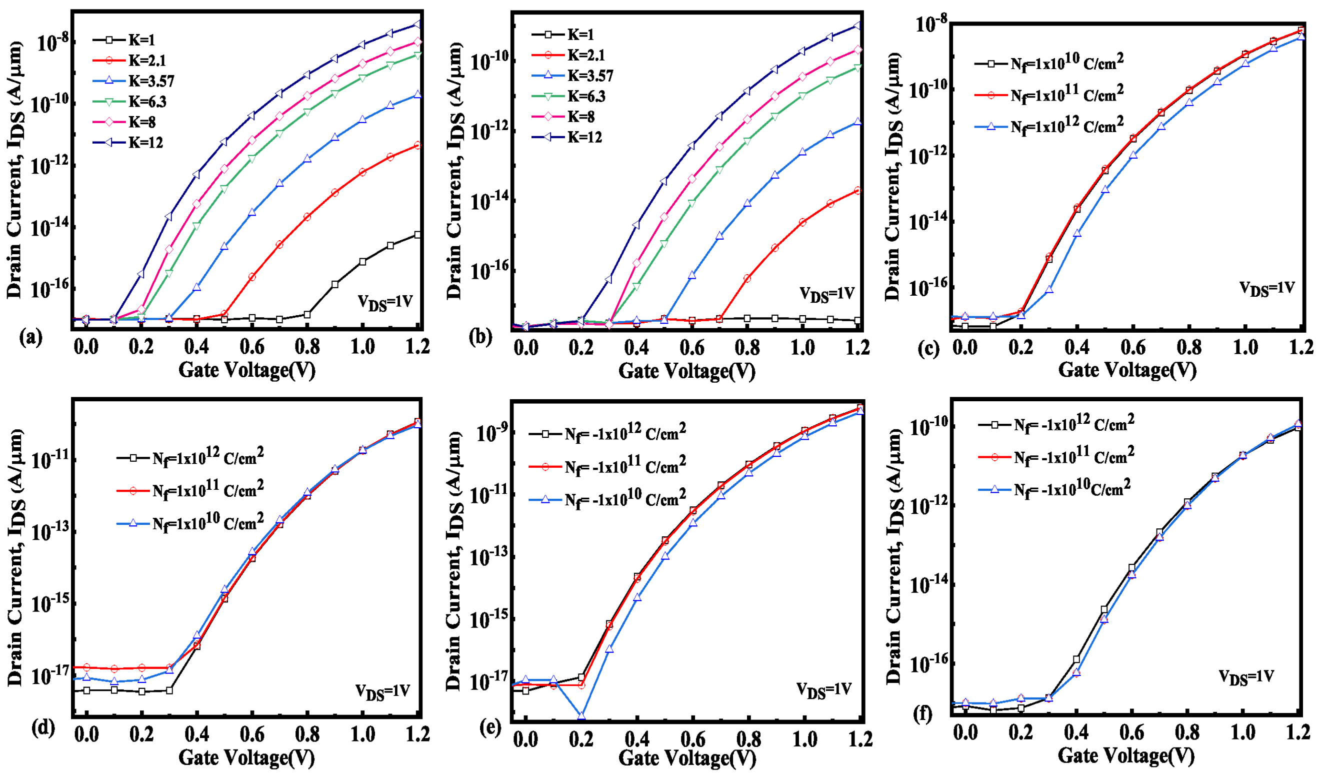

Fig. 8: Transfer characteristics of FE-CP-TFET based biosensor (a) with cavity height $h_c$ = 2.5 nm of neutral biomolecules; (b) with cavity height $h_c$ = 5.5 nm for neutral biomolecules; (c) with cavity height $h_c$ = 2.5 nm for positive charged biomolecules; (d) with cavity height $h_c$ = 5.5 nm for positive charged biomolecules; (e) with cavity height $h_c$ = 2.5 nm for negative charged biomolecules; and (f) with cavity height $h_c$ = 5.5 nm of negative charged biomolecules.

TABLE III: Sensitivity parameter values of FE-CP-TFET based biosensor with cavity length $h_c$ = 2.5 nm and $h_c$ = 5.5 nm due to positive and negative charged biomolecules.

| Employed biomolecules | Dielectric constant (K) and Charge density ($N_f$) | Proposed structure 1 Sensitivity ($S_I$) | Proposed structure 1 $I_{ON}/I_{OFF}$ Sensitivity | Proposed structure 2 Sensitivity ($S_I$) | Proposed structure 2 $I_{ON}/I_{OFF}$ Sensitivity |
|---|---|---|---|---|---|
| Positive Charged Biomolecules ($+N_f$) | K = 6, $N_f$ = $10^{10}$ C/$cm^2$ | $1.08\times10^6$ | $1.62\times10^6$ | $1.3\times10^7$ | $1.01\times10^7$ |
| | K = 6, $N_f$ = $10^{11}$ C/$cm^2$ | $1.06\times10^6$ | $6.82\times10^6$ | $1.29\times10^7$ | $3.78\times10^6$ |
| | K = 6, $N_f$ = $10^{12}$ C/$cm^2$ | $6.69\times10^5$ | $5.16\times10^5$ | $1.08\times10^7$ | $2.31\times10^6$ |
| Negative Charged Biomolecules (-$N_f$) | K = 6, $N_f$ =-$10^{10}C/cm^2$ | $7.79\times10^5$ | $7.05\times10^5$ | $1.3\times10^7$ | $3.76\times10^6$ |
| | K = 6, $N_f$ = -$10^{11}$ C/$cm^2$ | $1.03\times10^6$ | $1.3\times10^6$ | $1.31\times10^7$ | $3.87\times10^6$ |
| | K = 6, $N_f$ = -$10^{12}$ C/$cm^2$ | $1.05\times10^6$ | $2.17\times10^6$ | $1.31\times10^7$ | $6.31\times10^6$ |

TABLE IV: Sensitivity comparison of FE-CP-TFET based biosensor with other reported TFET biosensors.

| S.No. | TFET Based Biosensors | Sensitivity |
|---|---|---|
| 1. | Dielectric Modulated Electrostatically [42] doped TFET | $10^8$ |
| 2. | Vertical dielectrically modulated TFET [43] | $10^2$ |
| 3. | Electrically doped TFET [44] | $10^5$ |
| 4. | TFET with buried strained $Si_{(1-x)}Ge_x$ source structure [47] | $10^5$ |
| 5. | $N^+$ pocket doped Vertical TFET [48] | $10^6$ |
| 6. | Proposed Structure 1 | $6\times10^7$ |
| 7. | Proposed Structure 2 | $10^8$ |

the proposed structures, respectively. Fig. 12 shows the impact of variation of K value corresponding to different neutral biomolecules on the $I_{ON}$ and $I_{ON}/I_{OFF}$ sensitivity of both the proposed structures. An increment in the K value leads to improve the $I_{ON}$ current, hence $I_{ON}$ to $I_{OFF}$ sensitivity also improves. With the increased value of K, the coupling between source metal and source region gets enhanced more for the device with $h_c$ = 2.5 nm compared to the device with cavity height $h_c$ = 5.5 nm. Hence, the device with a lower cavity height shows a greater $I_{ON}$ current as described in Fig. 10. The maximum $I_{ON}$ is achieved by the device with $h_c$ = 2.5 nm is 3.76 $\times10^{-8}$ A/$\mu$m. Moreover, in OFF state condition the tunneling barrier width towards source-channel junction is larger in the biosensor with cavity height $h_c$ = 5.5 nm as compared to the other device leads to a lower $I_{OFF}$ value of approximately 2.56 $\times10^{-18}$ A/$\mu$m and 9.97 $\times10^{-18}$ A/$\mu$m for low cavity height structure irrespective of K value. Thus, the highest $I_{ON}/I_{OFF}$ sensitivity of $1.45\times10^8$ for K

This article has been accepted for publication in a future issue of this journal, but has not been fully edited. Content may change prior to final publication. Citation information: DOI 10.1109/TNB.2022.3174266, IEEE Transactions on NanoBioscience



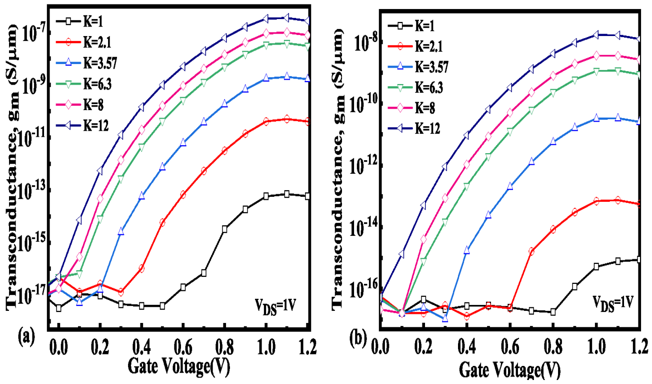


Fig. 9: Transconductance of FE-CP-TFET based biosensor (a) with cavity height $h_c$ = 2.5 nm of neutral biomolecules, and (b) with cavity height $h_c$ = 5.5 nm of neutral biomolecules.

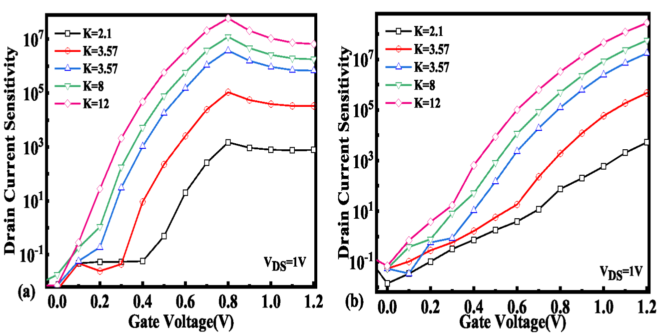


Fig. 10: Drain current sensitivity of FE-CP-TFET based biosensor (a) with cavity height $h_c$ = 2.5 nm for neutral biomolecules, and (b) with cavity height $h_c$ = 5.5 nm for neutral biomolecules.

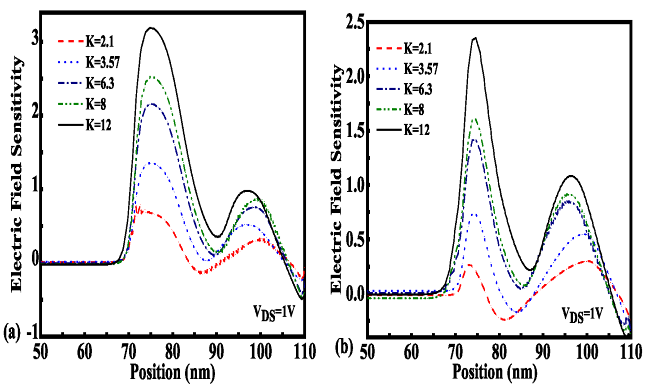


Fig. 11: Electric field sensitivity of FE-CP-TFET based biosensor (a) with cavity height $h_c$ = 2.5 nm and (b) with cavity height $h_c$ = 5.5 nm.

= 12 for the proposed device with cavity height $h_c$ = 5.5 nm is achieved.

The reflections of various charged biomolecules (present in the cavity region) on the sensitivity values (drain current sensitivity, $E_F$ sensitivity, $I_{ON}/I_{OFF}$, and transconductance sensitivity ) are listed in TABLE. III. It is observed from the table, that the drain current sensitivity as well as $I_{ON}/I_{OFF}$

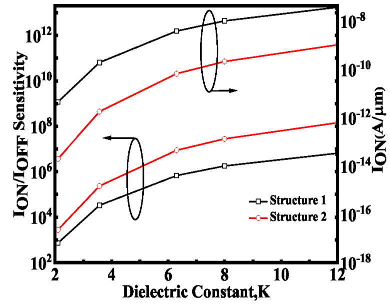


Fig. 12: Impact of dielectric constant of neutral biomolecules on $I_{ON}$ and $I_{ON}/I_{OFF}$ Sensitivity of FE-CP-TFET based biosensor with $h_c$ = 2.5 nm (Structure 1) and with $h_c$ = 5.5 nm (Structure 2).

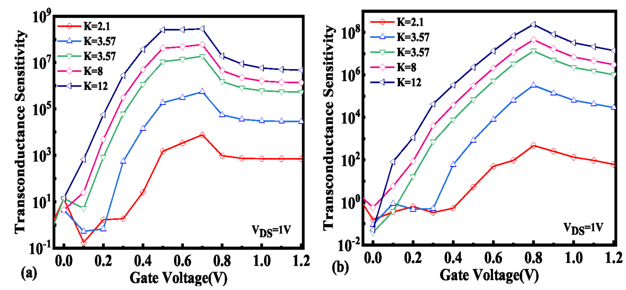


Fig. 13: Transconductance sensitivity of FE-CP-TFET based biosensor (a) with cavity height $h_c$ = 2.5 nm of neutral biomolecules, and (b) with cavity height $h_c$ = 5.5 nm of neutral biomolecules.

sensitivity of both the reported structure reduces with an increase in the positive charged biomolecules concentration. As positively charged biomolecules concentration reduces the tunneling rate at the source-channel junction. An opposite phenomenon is observed for the negatively charged biomolecules as it lowers the tunneling width to allow a large number of carriers to tunnel through it, which further enhances the drain current.

TABLE. IV summarizes the comparison of the sensitivity of the proposed work with various other TFET based biosensor devices that have been reported in the literature. The drain current sensitivity observed for the proposed structure is $\approx$ $6\times10^7$ which is lesser than the sensitivity reported in [42], but the proposed structure achieved this sensitivity comparatively at lesser supply voltage ($V_{GS}$ = 1.2 V) due to the incorporation of ferroelectric material. Moreover, it is evident that the proposed structure shows enhanced sensitivity than the other reported works as the cavity carved beneath the gate source electrode and also the cavity length is larger than the ref. [44] and [48]. In comparison to reported work in [43], [47], the sensitivity is significantly higher owing to the suppressed OFF current in the proposed structure. Finally, transconductance sensitivity of the proposed structures has been investigated for the neutral biomolecules as shown in Fig. 13. An increase in dielectric constant of the neutral biomolecules increases the transconductance sensitivity and it has achieved the maximum value of the order of $10^8$ for both the structures.

This article has been accepted for publication in a future issue of this journal, but has not been fully edited. Content may change prior to final publication. Citation information: DOI 10.1109/TNB.2022.3174266, IEEE Transactions on NanoBioscience



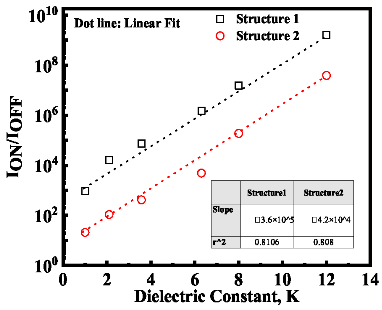


Fig. 14: $I_{ON}/I_{OFF}$ linearity for dielectric constant varies from 1 to 12 of both the proposed structures.

### C. Linearity analysis of FE-CP-TFET based biosensor

Linearity is a vital FOM for the sensor application. It reflects the ability of a sensor to respond to changes in a variable to be measured similarly across the full range. In this work, the linearity of the proposed structure has been analyzed in terms of the shift in the $I_{ON}$ to $I_{OFF}$ ratio with the variation of the different dielectric constants of the biomolecules to be detected. The linearity equation for $I_{ON}$ to $I_{OFF}$ ratio sensitivity is given as $I_{ON}/I_{OFF}$ = slope[K]+ $I_{ON}/I_{OFF}$(K = 1). Pearson's coefficient($r^2$) is computed to examine the degree of fitness. $I_{ON}/I_{OFF}$ linearity of both the proposed structure with respect to dielectric constant (K=1 to K = 12) is shown in Fig. 14.

It is shown in the table inserted in Fig. 15 reveals that the $I_{ON}/I_{OFF}$ sensitivity for structure1 is of range 3.6 $\times 10^5$ per K value and $4.2\times10^4$ per K value for structure 2. The fitness coefficients for both the structures are found to be $r^2 \geq 0.8$. Subthreshold Swing (SS) and average SS of the device are evaluated with the Eqn. (10) and (11) expressed as:

$$SS = \frac{\partial V_{GS}}{\partial(\log_{10} I_D)} \tag{10}$$

$$SS_{avg} = \frac{V_T - V_{OFF}}{\log_{10} I_T - \log_{10} I_{OFF}} \tag{11}$$

For the proposed device the SS value, which is minimum $SS_{point}$ and average SS value have been achieved as 52.8 mV/decade and 91.6 mV/decade, respectively for the biomolecules having K = 12. Therefore after these critical analysis, It can be claimed that the proposed structure may be the better alternative to detect several biomolecules modulated by dielectric constant and charge property such as SARS-CoV-2 virus [55], different proteins and Amino acids [56].

## IV. Conclusion

The work reports a highly sensitive biosensor based on the dual cavity dielectric modulated ferroelectric charge plasma Tunnel FET (FE-CP-TFET). The cavity regions are carved at the source gate dielectric interfaces to get the steeper edge at source-channel junction and hence better electrical detection sensitivity. To precisely detect the bio-analytes the comparison of two structural variants (i.e. one with cavity height $h_c$ = 2.5 nm and another with $h_c$ = 5.5nm ) has been carried out. The charge plasma technique is utilized here to suppress the negative conduction and to improve the random dopant fluctuations (RDFs). Moreover, the negative capacitance (NC) effect has been incorporated with the sensing device to empower the low power operation for the detection of the target biomolecules. Two different figures-of-merit (FOMs) sensitivity analyses (in terms of drain current, $I_{ON}/I_{OFF}$, electric field, and transconductance sensitivity) and linearity analysis are demonstrated here. The impact of neutral and charged biomolecules trapped into the cavity region on these FOMs are considered as key sensing metrics of the proposed device. The maximum value of the drain current sensitivity is achieved as 2.76 $\times 10^8$, $EF$ sensitivity is reported as 3.5, $I_{ON}/I_{OFF}$ sensitivity is $1.45\times10^8$ and transconductance sensitivity is of the order of $10^8$ with $h_c$ = 5.5 nm for K = 12 at $V_{GS}$ = 1.2 V. Linearity analysis in terms of $I_{ON}/I_{OFF}$ of the structures achieved degree of fitness as $r^2 \geq 0.8$. Based on our study, reported biosensor can be a potential contender for future bio-sensing applications.

## Acknowledgement

All authors state that they have no competing financial interests or personal ties that could influence or be relevant to the work disclosed in this paper.

## References

[1] G. Marrazzaet, I. Chianella, and M. Mascini "Disposable DNA Electrochemical Sensor for Hybridization Detection," Biosensors and Bioelectronics, vol. 14, no. 1, pp. 43-51, Jan. 1999.

[2] J. P. Cloarec, F.Bessueille, , E. Souteyrand, J. R.Martin, and J.P.Chauvet, "Control of Immobilization and Hybridization on DNA Chips by Fluorescence Spectroscopy," J. Fluorescence, vol. 10, no. 3, pp. 247-253, Feb. 2000.

[3] M. M. Miller, P. E. Sheehan, R. L. Edelstein, C. R. Tamanaha, L. Zhong, S. Bounnak, L. J. Whitman, and R. J. Colton., "A DNA Array Sensor Utilizing Magnetic Microbeads and Magnetoelectronic Detection," J. Magnetism and Magnetic Materials, vol. 225, no. 2, pp. 138-144, Jan. 2001.

[4] S. Busse, V. Scheumann, B. Menges, and S. Mittler, "Sensitivity studies for specific binding reactions using the biotin/streptavidin system by evanescent optical methods," Biosensors and Bioelectronics, vol. 17, no. 8, pp. 704–710, 2002.

[5] T. G. Drummond, M. G. Hill, and J. K. Barton, "Electrochemical DNA sensors," Nature Biotechnology, vol. 21, no. 10, pp. 1192–1199, 2003.

[6] V. Nabaei, R. Chandrawati, and H. Heidari, "Magnetic biosensors: Modelling and simulation," Biosensors and Bioelectronics, vol. 103, no. November 2017, pp. 69–86, 2018.

[7] D. Y. Jang, Y. P.Kim, H. S. Kim, S. H. Ko Park, S. Y. Choi, and Y. K. Choi, "Sublithographic Vertical Gold Nanogap for Label-free Electrical Detection of Protein-ligand Binding," J. Vac. Sci. Technol. B. vol. 25, no. 2, pp. 443-447, Apr. 2007.

[8] X. Chen, Z. Guo, G.-M. Yang, J. Li, M.-Q. Li, J.-H. Liu, and X.-J. Huang, "Electrical nanogap devices for biosensing," Mater. Today, vol. 13, no. 11, pp. 28–41, Nov. 2010.

[9] B. J. Schaertel, Ruth Firstenberg eden, "Biosensors in the Food Industry: Present and Future,"J. Food Protection, vol. 51, no. 10, pp. 811-820, Oct. 1988.

[10] V. T. Nguyen, Y. S. Kwon, and M. B. Gu, "Aptamer-based Environmental Biosensors for Small Molecule Contaminants," Current Opinion Biotechnol., vol. 45, pp. 15-23, June 2017

[11] B. D. Malhotra, S. Kumar, and C. M. Pandey, "Nanomaterials Based Biosensors for Cancer Biomarker Detection," J. Phys., Conf. Ser., vol. 704, pp. 1-11, Apr. 2016.

[12] M. Barbaro, Bonfiglio A, RaffoL, "A charge-modulated FET for detection of biomolecular processes: conception, modeling, and simulation," IEEE Trans. Electron Devices, vol. 53, no. 1, pp. 158–166, 2006.

[13] C. H. Kim, C. Jung, H. G. Park, and Y. K. Choi, "Novel dielectric modulated field-effect transistor for label-free DNA detection," Bio Chip Journal, vol. 2, no. 2, pp. 127–134, 2008.

[14] D. Sarkar and K. Banerjee, "Proposal for tunnel-field-effect-transistor as ultra-sensitive and label-free biosensors," Applied Physics Letters, vol. 100, no. 14, 2012.

[15] S. Singh, P. N. Kondekar, and N. K. Jaiswal, "Label-free biosensor using nanogap embedded dielectric modulated schottky tunneling source impact ionization MOS," Microelectronic Engineering, vol. 149, pp. 129– 134, 2016.

[16] G. Wadhwa and B. Raj, "Parametric variation analysis of symmetric double gate charge plasma JLTFET for biosensor application," IEEE Sensors Journal, vol. 18, no. 15, pp. 6070–6077, 2018.

[17] P. Dwivedi and A. Kranti, "Applicability of transconductance-to-current ratio ( $g_m/i_{ds}$ ) as a sensing metric for tunnel FET biosensors," IEEE Sensors Journal, vol. 17, no. 4, pp. 1030–1036, 2017.

[18] S. O. Koswatta, M. S. Lundstrom, and D. E. Nikonov, "Performance comparison between p-i-n tunneling transistors and conventional MOSFETs," IEEE Trans. Electron Devices, vol. 56, no. 3, pp. 456–465, Mar. 2009. doi: 10.1109/TED.2008.2011934.

[19] D. Singh, S. Pandey, K. Nigam, D. Sharma, D. S. Yadav, and P. Kondekar, "A charge-plasma-based dielectric-modulated junctionless TFET for biosensor label-free detection," IEEE Trans. Electron Devices, vol. 67, no. 1, pp. 271–278, Jan. 2017.

[20] A. Hraziiaet al., "An analysis on the ambipolar current in Si double-gate tunnel FETs," Solid-State Electron., vol. 70, pp. 67– 72, Apr. 2012.

[21] S. Saurabh, M.J. Kumar, "Novel attributes of a dual material gate nanoscale tunnel field-effect transistor," IEEE Trans. Electron Devices, vol. 58, no. 2, pp. 404–410, 2010.

[22] S. Kanungo, S. Chattopadhyay, P. S. Gupta, K. Sinha, and H. Rahaman, "Study and analysis of the effects of SiGe source and pocket-doped channel on sensing performance of dielectrically modulated tunnel FET-based biosensors," IEEE Trans. Electron Devices, vol. 63, no. 6, pp. 2589–2596, Jun. 2016.

[23] B. R. Raad, D. Sharma, K. Nigam, and P. Kondekar, "Physics-based simulation study of highperformance gallium arsenide phosphide–indium gallium arsenide tunnel field-effect transistor," IET Micro Nano Lett., vol. 11, no. 7, pp. 366–368, Jul. 2016.

[24] B. R. Raad, K. Nigam, D. Sharma, and P. N. Kondekar, "Performance investigation of bandgap, gate material work function and gate dielectric engineered TFET with device reliability improvement," Superlattices Microstruct., vol. 94, no. 6, pp. 138–146, Jun. 2016.

[25] R. Vishnoi, M. J. Kumar, "Compact analytical drain current model of gate-all-around nanowire tunneling FET," IEEE Transactions on Electron Devices, vol.61, no. 7, pp. 2599-2603, 2014.

[26] L. Lattanzio, G. A. Salvatore, A. M. Ionescu, Non-hysteretic ferroelectric tunnel FET with improved conductance at curie temperature, Proc. Device Res. Conf.2010; 67–68.

[27] A. Saeidi, A. Biswas, A. M. Ionescu, "Modeling and simulation of low power ferroelectric non-volatile memory tunnel field effect transistors using silicondoped hafnium oxide as gate dielectric", Solid-State Electron, 124, pp. 16-23, 2016.

[28] M. Kumar, S. Jit, A Novel Four-Terminal Ferroelectric Tunnel FET for Quasi-Ideal Switch,IEEE Transactions on Nanotechnology, vol.14, no.4, pp. 600-602, 2015.

[29] A. M. Ionescu, L. Lattanzio, G. A. Salvatore, L. De Michielis, K. Boucart, D. Bouvet, The Hysteretic Ferroelectric Tunnel FET,IEEE Transactions on Electron Devices, vol. 57, no. 12, pp. 3518-3524, 2010.

[30] L. D. Landau , I. M. Khalatnikov, On the anomalous absorption of sound near a second order phase transition point, Dokl. Akad. Nauk SSSR vol. 96, pp.469–47, 1954.

[31] A. Saeidi, F. Jazaeri, I. Stolichnov, A.M. Ionescu Double-gate negative-capacitance MOSFET with PZT gate-stack on ultra-thin body SOI: An experimentally calibrated simulation study of device performance, IEEE Transactions on Electron Devices vol. 63, no. 12, pp. 4678-4684, 2016.

[32] J. Min, J. Wu, Y. Taur, "Analysis of source doping effect in tunnel FETs with staggered bandgap," IEEE Electron Device Lett, vol. 34, no. 10, pp. 1094–1096, 2015.

[33] C. Sandow, J. Knoch, C. Urban, Q. T. Zhao, S. Mant, "Impact of electrostatics and doping concentration on the performance ofsilicon tunnel field-effect transistors,"Solid State Electron,vol. 53, no. 10, pp. 1126–1129, 2009.

[34] S. Agarwal, G. Klimeck, and M. Luisier, "Leakage-reduction design concepts for low-power vertical tunneling field-effect transistors," IEEE Electron Device Lett., vol. 31, no. 6, pp. 621– 623, Jun. 2010.

[35] S. Singh and P.N. Kondekar, "Circuit Performance & Sensitivity Analysis of Charge Plasma based Super-Steep Negative Capacitance Junctionless Tunnel Field Effect Transistor, Journal of Nanoelectronics and Optoelectronics, 12, no. 5, pp. 442-451, 2017.

[36] S. Singh, P. Pal, P. N. Kondekar, "Charge-plasma-based super-steep negative capacitance junctionless tunnel field effect transistor: design and performance", IET Electronics Letters, vol. 50(25), pp. 1963-1965, 2014.

[37] M. J. Kumar and S. Janardhanan, "Doping-less tunnel field effect transistor: Design and investigation," IEEE Trans. Electron Devices, vol. 60, no. 10, pp. 3285–3290, Oct. 2013.

[38] A. Kaity, S. Singh, P.N. Kondekar, "Silicon-on-nothing electrostatically doped junctionless tunnel field effect transistor (SON-ED-JLTFET): a short channel effect resilient design," Silicon, vol. 13, no. 1,pp. 9-23, 2021.

[39] ATLAS, "Device Simulation Software," Silvaco Int.,Santa Clara,CA,USA, 2016.

[40] P. C. Adell, H. J. Barnaby, R. D. Schrimpf, and B. Vermeire, "Band-to- Band Tunneling (BTBT) induced leakage current enhancement in irradiated fully depleted SOI devices," IEEE Transactions on Nuclear Science, vol. 54, no. 6, pp. 2174–2180, 2007.

[41] A. M. Ionescu and H. Riel, "Tunnel field-effect transistors as energy efficient electronic switches," Nature, vol. 479, no. 7373, pp. 329–337, 2011.

[42] P. Venkatesh, K. Nigam, S. Pandey, D. Sharma, and P. N. Kondekar, "A dielectrically modulated electrically doped tunnel FET for application of label free biosensor," Superlattices and Microstructures, vol. 109, pp. 470–479, 2017.

[43] M. Verma, S. Tirkey, S. Yadav, D. Sharma, and D. S. Yadav, "Performance Assessment of A Novel Vertical Dielectrically Modulated TFET Based Biosensor," IEEE Transactions on Electron Devices, vol. 64, no. 9, pp. 3841–3848, 2017.

[44] D. Sharma, D. Singh, S. Pandey, S. Yadav, and P. N. Kondekar, "Comparative analysis of full-gate and short-gate dielectric modulated electrically doped Tunnel-FET based biosensors," Superlattices and Microstructures, vol. 111, pp. 767–775, 2017.

[45] K. Boucart and A. M. Ionescu, "Double-gate tunnel FET with high-k gate dielectric," IEEE Trans. Electron Devices, vol. 54, no. 7, pp. 1725–1733, Jul. 2007.

[46] P. M. Solomon et al., "Universal tunneling behavior in technologically relevant P/N junction diodes," J. Appl. Phys., vol. 95, no. 10, pp. 5800–5812, 2004.

[47] A. Anam, S. Anand and S. I. Amin, "Design and Performance Analysis of Tunnel Field Effect Transistor with Buried Strained $Si_{1-x}Ge_x$S ource Structure Based Biosensor for Sensitivity Enhancement", IEEE Sens. J, vol. 20, no. 22, pp. 13178-13185, Jun. 2020.

[48] V. D. Wangkheirakpam, B. Bhowmick, and P. D. Pukhrambam, $N^+$ Pocket Doped Vertical TFET Based Dielectric-Modulated Biosensor Considering Non-Ideal Hybridization Issue: A Simulation Study, IEEE Transactions on Nanotechnology, 19, pp. 156-162, 2020.

[49] S. Singh, A.K.S. Chauhan, G. Joshi, J. Singh, Design and Investigation of SiGe Heterojunction Based Charge Plasma Vertical TFET for Biosensing Application, Silicon:1–12, 2021.

[50] Clima S, Wouters DJ, Adelmann C, Schenk T, Schroeder U, Jurczak M, Pourtois G (2014) Identification of the ferroelectric switching process and dopant dependent switching properties in orthorhombic $HfO_2$; A first principles insight, vol 104

[51] D. Kwon, S. Cheema, N. Shanker, K. Chatterjee, Y.H. Liao, A. J. Tan, C. Hu, S. Salahuddin,"Negative capacitance FET With 1.8- nm-Thick Zr-Doped HfO2 Oxide," IEEE Electron Device Letters, vol. 40, no.6, pp.993–996, 2019.

[52] G. M. Hurkx, D. M. Klaassen, and M. G. Knuvers, "A new recombination model for device simulation including tunneling," IEEE Trans. Electron Devices, vol. 39, no. 2, pp. 331–338, Feb. 1992.

[53] S. Salahuddin, "Use of negative capacitance to provide voltage amplification for low power nanoscale devices," Nano Lett. vol. 8, no. 2, 2008.

[54] Q. Zhang, W. Zhao, A. Seabaugh, "Low-subthreshold-swing tunnel transistors," IEEE Electron. Device Lett. 27,2006.

[55] K.N. Priyadarshani, S. Singh, and M.K. Mohammed, "Gate-all-around junctionless FET based label-free dielectric/charge modulation detection of SARS-CoV-2 virus", RSC Advances, vol. 12, no. 15, pp. 9202-9209, 2022.

[56] H. Bharadwaj, N. Kumar, S. I. Amin, and S. Anand, "Charge Plasma Based Vertical Nanowire Tunnel Field Effect Transistor: Design and Sensitivity Analysis for Biosensing Application", Silicon, pp. 1-8, 2021